

COMBINED ANALYSIS OF OPTICAL AND SAR REMOTE SENSING DATA FOR FOREST MAPPING AND MONITORING

E. LEHMANN¹, Z.-S. ZHOU¹, P. CACCETTA¹, A. MITCHELL², A. MILNE²,
K. LOWELL³, S. MCNEILL⁴

¹*CSIRO Mathematics, Informatics & Statistics, Floreat, Western Australia –
{eric.lehmann, zheng-shu.zhou, peter.caccetta}@csiro.au*

²*CRC-SI, University of New South Wales, Sydney, Australia –
{a.mitchell, t.milne}@unsw.edu.au*

³*CRC-SI, University of Melbourne, Australia – klowell@unimelb.edu.au*

⁴*Landcare Research, Lincoln, New Zealand – mcneills@landcareresearch.co.nz*

ABSTRACT

Jointly processing remote sensing (RS) data acquired by sensors operating at different wavelengths offers the potential to significantly improve the operation of global forest mapping and monitoring systems. This paper presents an analysis of the forest discrimination properties of optical imagery (Landsat TM) and synthetic aperture radar (SAR) data acquired at L-band (ALOS-PALSAR) and C-band (RADARSAT-2), when considered either separately or as a combined source of information. This pilot study is carried out over a test site in north-eastern Tasmania, Australia. Canonical variate analysis, a directed discriminant technique, is used to investigate the separability of a number of training sites, which are subsequently used to define spectral classes for maximum likelihood classification. An accuracy assessment of the forest classification results is provided on the basis of independent validation data. A variable selection is also performed, producing quantitative metrics on the degree of land cover separation provided by various combinations of the SAR and optical bands. The experimental results highlight the advantages of combining multi-sensor RS data for purposes such as natural resources and land management, environmental assessment, and carbon accounting.

1. INTRODUCTION

The use of RS data provides an important source of information for environmental monitoring, as demonstrated in many application fields ranging from conservation and natural resources management [1] to carbon accounting [2]. Recent technological advances have also allowed the deployment of many new RS satellites, particularly in the field of SAR. In parallel, the development of robust methods for large-scale forest monitoring is also becoming increasingly important. The joint analysis of multi-sensor data can potentially improve the operation of environmental monitoring systems significantly.

The need for global forest monitoring systems is demonstrated by the recent launch of several multi-governmental initiatives such as the Forest Carbon Tracking task of the Group on Earth Observations (GEO-FCT, www.geo-fct.org). In response to GEO-FCT, the Australian Department of Climate Change and Energy Efficiency (DCCEE) launched the International Forest Carbon Initiative (IFCI), which aims to increase international forest carbon monitoring and accounting capacity in accordance with emerging international reporting and verification requirements. Land cover monitoring systems based on optical RS data have been operational for many years in several parts of the world. In Australia, the National Carbon Accounting System (NCAS [2], [3]) offers the capability for fine-scale continental mapping and monitoring of the extent and change in perennial vegetation using Landsat satellite imagery, allowing for an effective estimation of the greenhouse gas emissions from land use and land use changes [4]. Among others, future developments of the NCAS framework under IFCI involve taking advantage of new technologies in the area of spaceborne SAR sensors.

An important step towards multi-sensor environmental monitoring is to address the key aspect of sensor complementarity (adding thematic value by using more than one sensor), and thus to quantify the performance gains achievable by using a SAR–optical data fusion approach. This article demonstrates the potential use of combined optical and SAR data for the purpose of forest monitoring, and presents a quantitative analysis and comparison of the forest/non-forest (F/NF) discrimination results. It reports some of the findings obtained from the work carried out in the frame of Australia's contribution to the GEO-FCT initiative.

2. DATA AND STUDY AREA

2.1. Study Area

This work is part of a pilot study carried out for a 66km×50km demonstration area in north-eastern Tasmania, Australia (Figure 1, left), which includes one of Australia's national calibration sites defined in the frame of the GEO-FCT initiative. It contains a variety of land covers including rainforests, wet and dry eucalypt forests, non-eucalypt forests, pine and eucalypt plantations, agricultural land, as well as treeless alpine and moorland vegetation. Significant topographic variations can also be found across the study site with the terrain elevation varying between 85m and 1510m above sea level.

2.2. ALOS-PALSAR Data

The ALOS-PALSAR data in this study were acquired at L-band (~23.6cm wavelength) in fine-beam dual-polarisation mode (HH and HV), in an ascending orbit with off-nadir angle of 34.3°. In the study area, the data is a mosaic of two PALSAR scenes, namely scene 381/6340 in the west (acquired on 07 Oct. 2009) and scene 380/6340 in the east (acquired on 20 Sept. 2009). The single-look complex data (SLC level 1.1) was pre-processed according to the following steps: 1.) 8×2 multi-looking (range × azimuth) resulting in a 29.8m×25.1m pixel size, 2.) speckle filtering with 5×5 Lee filter, 3.) radiometric calibration and normalisation, 4.) geocoding to 25m pixel size to match the Landsat resolution, using a digital elevation model (DEM) with 25m cell resolution, 5.) terrain illumination correction using the 25m DEM, and 6.) gradient mosaicing of the two scenes. The result is a mosaic of orthorectified, terrain-corrected and radiometrically calibrated PALSAR data at 25m resolution (Figure 1, centre-left). The terrain correction step is necessary to compensate for illumination differences due to the topographical variations and side-looking orientation of the SAR sensor. This correction was carried out using the

algorithm described in [5], which considers the SAR scattering in forested areas together with the local slope angles to derive the terrain correction coefficients.

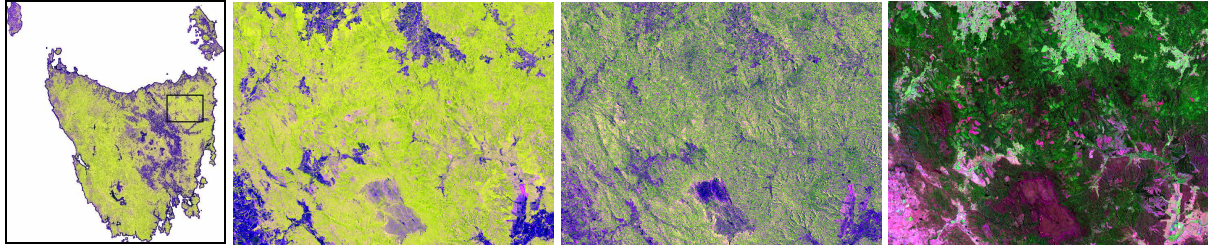


Figure 1: SAR and optical datasets. *Left to right*: PALSAR mosaic over Tasmania (the box shows the 66km×50km area of interest); PALSAR data (σ° in dB) for the study area, HH/HV/HH-HV in R/G/B; RADARSAT-2 data (σ° in dB), VV/VH/VV-VH in R/G/B; and Landsat-TM data, bands 5/4/2 in R/G/B.

2.3. RADARSAT-2 Data

The C-band data (~5.6cm wavelength) used here was acquired by the RADARSAT-2 sensor in wide-beam (W3) dual-polarisation mode (VV and VH) with an incidence angle of 42.2° in ascending orbit. The data covering the study area is part of a scene acquired on 07 Sept. 2009. Data pre-processing was carried out in a manner similar to that used for the PALSAR data (see Section 2.2). Here, the multi-looking step used 1 range look and 4 azimuth looks (resulting ground pixel size: 17.6m×25.7m), and no mosaicing was necessary. The resulting C-band data is shown in Figure 1 (centre-right).

2.4. Landsat-TM Data

Optical data was obtained from the existing archive of calibrated Landsat MSS/TM/ETM+ images produced as part of Australia's NCAS program [2]. Within this framework, each Landsat scene was processed according to the following steps: 1.) orthorectification to a common spatial reference, 2.) top-of-atmosphere reflectance calibration (sun angle and distance correction), 3.) correction of scene-to-scene differences using bi-directional reflectance distribution functions, 4.) calibration to a common spectral reference using invariant targets, 5.) terrain illumination correction, 6.) removal of corrupted data (e.g. regions affected by smoke, clouds and sensor deficiencies), and 7.) mosaicing of individual Landsat scenes into 1:1,000,000 map sheets. Key aspects of this processing are discussed in [2] and full operational details are given in [3]. The data covering the study area was acquired on 17 Jan. 2009 (scene 090/88), with data from Feb. 2009, Mar. 2009 and Feb. 2010 used as fill-in in cloud-affected areas (~18% of the image). The resulting Landsat mosaic is shown in Figure 1 (right).

2.5. Data Coregistration

Ideally, accurate coregistration between the optical and SAR images would be established with the use of cross-correlation techniques, image to image registration, and a common DEM in order to achieve sub-pixel alignment. Here, a common DEM was used but the SAR data was orthorectified using the sensors' orbital parameters while the Landsat data was taken from the legacy NCAS system, which used historic state topographic mapping as primary control. The coregistration between datasets was therefore assessed with the use of a gradient cross-correlation technique [6], which provides sub-pixel assessment results by detecting and matching features in the two images being compared.

The PALSAR–Landsat coregistration was assessed using 127 ground features, leading to an accuracy of 0.56 pixel (25m pixel size) with 96% of the residuals below 1.5 pixels, and with no apparent signs of systematic spatial deviations between the two images. The RADARSAT-2 data was originally found to

be poorly coregistered with the Landsat image (south-east shift of about 2.4 pixels); the RADARSAT-2 image was thus re-registered to the optical data. The increased speckle in the RADARSAT-2 image produced more variability in the coregistration results, here only allowing 90 ground features to be used for the assessment. The average displacement of the re-registered RADARSAT-2 data compared to Landsat was found to be 1.05 pixels with about 74% of the residuals below 1.5 pixels. Based on these results, the datasets' coregistration was considered satisfactory for joint SAR–optical processing.

2.6. Reference Data

Selection of the training and validation sites for the following analyses was based on a consideration of SPOT imagery (2.5m resolution) and a vegetation map product (TASVEG) from the state of Tasmania. In the area of interest, the SPOT image was a mosaic of four scenes acquired between Nov. 2009 and Feb. 2010. The TASVEG map was used to obtain land cover information, and the SPOT data provided an added check on whether the cover had deviated or changed from the TASVEG label. TASVEG is a Tasmania-wide vegetation map produced by the Tasmanian Vegetation Mapping and Monitoring Program within the Department of Primary Industries and Water (www.thelist.tas.gov.au). It comprises 154 distinct vegetation communities mapped at a scale of 1:25,000, and provides a reference that can be used for a broad range of management and reporting applications relating to vegetation in Tasmania. This information is based on a combination of field observations, photo-interpretation and information from other sources such as geological maps and permanent inventory plots. TASVEG is continually revised and updated to reflect changes in the natural environment. In the study area, field work for revision mapping started in Mar. 2005 and was completed in Oct. 2008. The selection of training and validation data was also done in conjunction with the optical and SAR imagery so as to minimise potential errors due to the different acquisition times of the reference data.

3. FOREST/NON-FOREST CLASSIFICATION

The F/NF discrimination analyses were applied to the following datasets: 1.) Landsat (six spectral bands, thermal band omitted), 2.) PALSAR (L-band, HH and HV), 3.) RADARSAT-2 (C-band, VV and VH), and 4.) combined SAR–optical data obtained by concatenating the Landsat, PALSAR and RADARSAT-2 bands (ten spectral bands). Using the reference data, 268 training sites (each approximately 150 to 200 pixels in size) were selected for the classifications so as to represent a broad range of land covers over the study area. The same training sites were used for all datasets, but aggregated separately in each analysis.

3.1. Definition of Spectral Classes

Using the training data, canonical variate analysis (CVA) produces a set of orthogonal linear basis functions (canonical vectors, CVs) based on maximising the ratio of between-class separation to within-class variance [7]. The metrics and plots produced by this technique provide information on whether to group or not to group certain sites. The analysis also indicates how reliably the selected sub-classes may be separated. For each of the SAR and optical datasets, CVA was used to aggregate the training sites into a number of sub-classes to reflect the common spectral characteristics of different land covers. Figure 2 shows the CVA plot obtained for the Landsat data, with the sites displayed in the space defined by the first two CVs. This figure also shows four sub-classes selected for this data, with labels identifying the land cover types represented by these groupings.

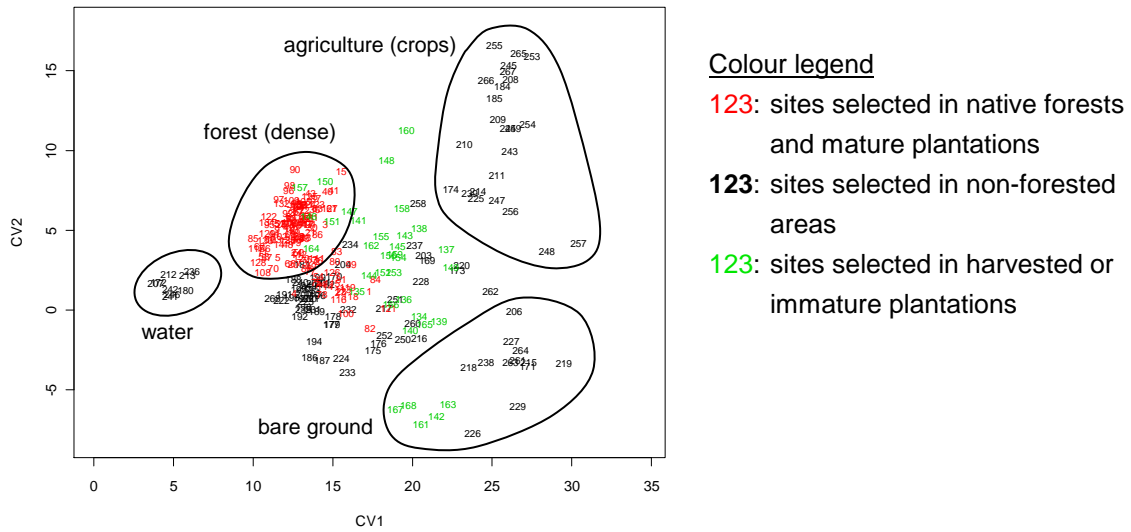


Figure 2: CVA plot for the Landsat data, showing four of the selected seven sub-classes (three more classes selected among the remaining sites).

The number of selected sub-classes reflects the ability of each dataset to discriminate between different land covers. A total of seven sub-classes could be identified for Landsat, six for PALSAR, four for RADARSAT-2, and eight for the combined SAR–optical dataset. Table 1 shows a list of these sub-classes, providing information as to which land cover types are separable based on each data. It must be noted that sites from the ‘immature plantations’ sub-class were here assigned to the non-forest category, due to their “bare ground” appearance in the Landsat and SPOT imagery; plantation sites were defined as mature when presenting a closed/dense canopy. Also, some separation appeared possible between native forests and certain ‘mature plantations’ sites in the SAR and optical data. This was however not investigated further due to a lack of accurate ground information regarding plantation types (hardwood vs. softwood) and age of the forestry stands in the study area.

	Landsat TM	PALSAR L-band	RADARSAT-2 C-band	Combined SAR–optical
Forest	1. dense forest (native and plantations) 2. sparse forest	1. dense forest (native and plantations) 2. mix of dense and sparse forest	1. (*) mix of sparse and dense forest (native and plantations), and harvested/immature plantations	1. dense forest (native and plantations) 2. sparse forest
Non-forest	3. water 4. agriculture (crops) 5. mix of agriculture (bare) and immature plantations 6. mix of alpine and Buttongrass vegetation 7. generic bare ground	3. water 4. generic agriculture 5. Buttongrass moorland 6. mix of alpine treeless vegetation and immature plantations	2. water 3. Buttongrass moorland 4. generic non-forest (agriculture and alpine treeless vegetation)	3. water 4. agriculture (crops) 5. immature plantations 6. Buttongrass moorland 7. alpine treeless vegetation 8. generic bare ground

Table 1: definition of sub-classes based on a CV analysis of the training data. (*) Note: the first class for the RADARSAT-2 data corresponds to a mix of forest and non-forest (immature plantations) sites.

3.2. Maximum Likelihood Classification

The spectral groupings identified in the previous section provided the classes used for a contextual maximum likelihood classifier (MLC), which produces a sub-class label image based on the input data

[8]. Maximum likelihood classification was used due to its ability to provide distance metrics related to the separation of the selected sites and sub-classes.

A quantitative assessment of the F/NF classifications was carried out on the basis of 204 validation sites uniformly distributed over the study area and selected independently of the training data. For this assessment, the multi-class MLC outputs were collapsed into forest and non-forest labels according to the definitions given in Table 1. Table 2 presents the resulting classification accuracy and confusion matrices as the percentage of validation sites mapped to the forest and non-forest classes by the MLC.

true labels	Landsat		PALSAR		RADARSAT-2		SAR-optical	
	F	NF	F	NF	F	NF	F	NF
F	60.78%	5.88%	64.22%	2.45%	64.71%	1.96%	61.27%	5.39%
NF	4.41%	28.92%	3.92%	29.41%	13.24%	20.10%	3.92%	29.41%
Accuracy	89.70%		93.63%		84.81%		90.68%	

Table 2: F/NF classification percentages (confusion matrices) of MLC outputs given the true labels.

These results show good classification accuracy (~90%) for the Landsat, PALSAR and combined SAR-optical data, with significantly lower results obtained with the RADARSAT-2 data. The slightly decreased accuracy achieved by the combined SAR-optical data compared to PALSAR is due to the intrinsic variability of the validation results (error margin) rather than major differences between the F/NF classifications, as can be seen in Figure 3. This figure shows the multi-class MLC outputs for a subset of the study area, and clearly demonstrates the superiority of the combined dataset (bottom-right image) in classifying land covers, especially regarding the separation of the Buttongrass moorland (yellow areas in the north-east corner of the plots) from the alpine vegetation (south-west corner).

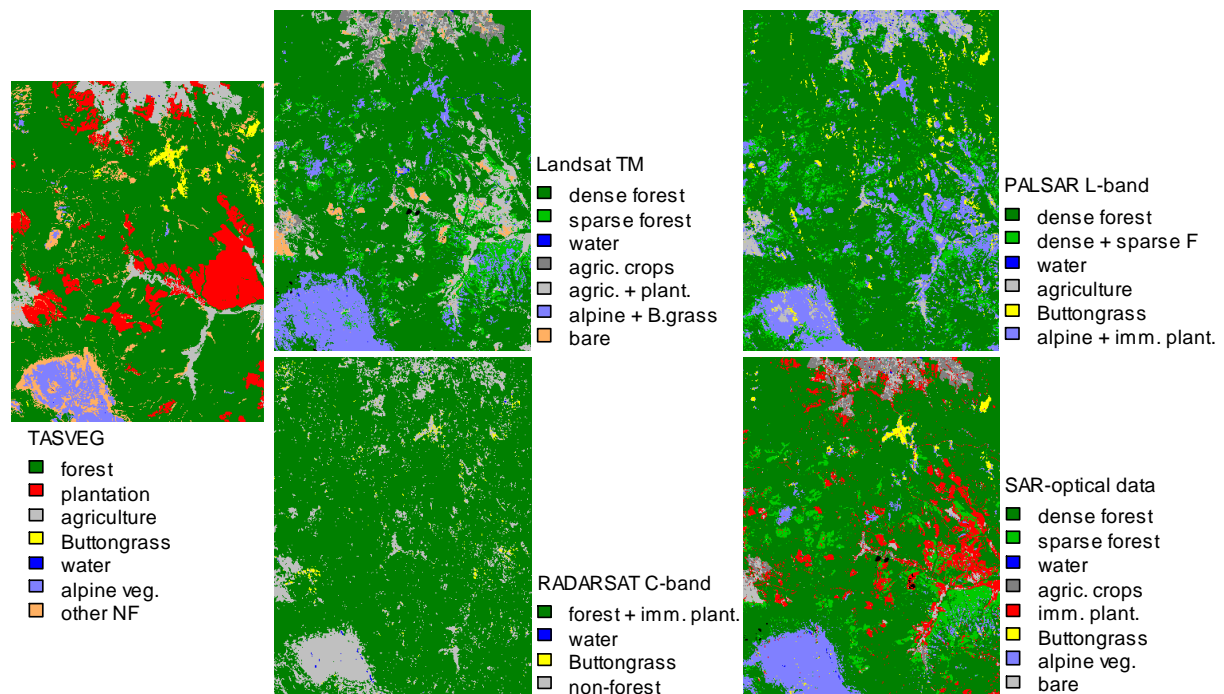


Figure 3: multi-class MLC outputs over a 25km x 33km subset of the study area, for the Landsat data (top-centre), PALSAR data (top-right), RADARSAT-2 data (bottom-centre) and combined SAR-optical dataset (bottom-right). The image on the left shows the reference data (TASVEG), with plantation areas shown in red regardless of their state (harvested, re-planted or mature).

3.3. Band Information

Another aspect of interest for multi-sensor integration is to examine the level of information provided by different combinations of the optical and SAR bands; this is achieved here by performing a variable selection analysis [9]. Table 3 presents the results as the percentage of discrimination provided by various subsets of bands with respect to the information available when all bands are considered simultaneously. This assessment is furthermore performed for three different scenarios used to check the separation existing between different sub-classes of training data (using the class aggregations defined for the combined SAR–optical dataset, see Table 1, last column).

The column labelled ‘Forest vs. non-forest’ in Table 3 presents generic discrimination results when all the forest sites are compared (contrasted) to all the non-forest sites (sites from the ‘water’ sub-class were removed from this analysis due to their clearly-separable spectral signatures). This column indicates that the optical data contains an equivalent of 57.29% of the F/NF discrimination information, while the PALSAR data on its own would provide 66.32% of this information and the RADARSAT-2 data 5.21%. In the case of PALSAR, most of the F/NF information (66.32%) is available from the HV polarisation alone (66.28%), while most of the RADARSAT-2 discrimination (5.21%) is available from the VH band (5.13%). This dependence on the cross-polarised bands is likely due to the influence of volumetric SAR scattering in forested areas. Finally, this example also shows that considering all the available data jointly leads to a significantly increased ability to separate the forest and non-forest sites (with an increase of at least 33% compared to using the optical or SAR data alone), thus demonstrating the complementary nature of the information provided by the SAR and optical sensors.

Bands	Forest vs. non-forest	Contrast 1	Contrast 2
PALSAR HH	17.33%	10.68%	5.95%
PALSAR HV	66.28%	30.29%	15.97%
PALSAR HH+HV	66.32%	30.76%	16.24%
RADARSAT-2 VV	0.25%	6.35%	0.41%
RADARSAT-2 VH	5.13%	24.95%	0.27%
RADARSAT-2 VV+VH	5.21%	25.69%	0.41%
TM (6 bands)	57.29%	40.88%	93.37%
TM+SAR (10 bands)	100.00%	100.00%	100.00%

Table 3: percentage of the discrimination information provided by different combinations of the optical and SAR bands (compared to using all available bands).

The last two columns in Table 3 contain results related to the discrimination between the least separable forest class (‘sparse forest’ in Table 1) and the two spectrally closest clusters of non-forest sites. The column labelled ‘Contrast 1’ corresponds to a contrast between ‘sparse forest’ and ‘alpine vegetation’, with the results leading to conclusions similar to those discussed above for the ‘Forest vs. non-forest’ contrast. The column ‘Contrast 2’ results from contrasting ‘sparse forest’ against the ‘immature plantations’ class. In this particular case, most of the discrimination is provided by the optical data, thus indicating a relative inability to separate these ground covers using the SAR data alone. This is likely the result of forestry logging and planting practices in this region of Tasmania, where debris (branches, logs, etc.) are often left on the ground following the harvesting of a plantation and subsequent planting of new seedlings (thus generating a strong cross-polarised backscatter). This observation is also in keeping with the class definitions shown in Table 1, where ‘immature plantations’

sites are always part of a mixture with other types of land cover for the PALSAR and RADARSAT-2 data (similar spectral signatures).

4. CONCLUSION

This paper investigated the forest discrimination properties of combined SAR and optical data. Significant classification improvements resulted from the combined data in comparison to using Landsat, L-band SAR (PALSAR) or C-band SAR (RADARSAT-2) independently. A variable selection analysis also showed a varying degree of discrimination provided by each of the SAR and optical bands, depending on the considered land cover types. The results also generally point to a significantly increased forest mapping capacity of the L-band SAR data compared to C-band. All the results presented in this work highlight the complementary nature of SAR and optical sensors for the purpose of forest mapping and monitoring. This paper also demonstrated how existing statistical methods (such as canonical variate analysis, variable selection and maximum likelihood classification) can be used as efficient investigation/classification tools so as to take full advantage of these complementary datasets.

REFERENCES

- [1] J. Wallace, G. Behn, and S. Furby, "Vegetation condition assessment and monitoring from sequences of satellite imagery," *Ecological Management and Restoration*, vol. 7, no. 1, pp. 31–36, Jun. 2006.
- [2] P. Caccetta, R. Waterworth, S. Furby, and G. Richards, "Monitoring Australian continental land cover changes using Landsat imagery as a component of assessing the role of vegetation dynamics on terrestrial carbon cycling," in *European Space Agency Living Planet Symposium*, pp. 1–7, Bergen, Norway, June-July 2010.
- [3] S. Furby, *Land cover change: specification for remote sensing analysis*. National Carbon Accounting System, technical report no. 9, Australian Greenhouse Office, Canberra, 2002.
- [4] C. Brack, G. Richards, and R. Waterworth, "Integrated and comprehensive estimation of greenhouse gas emissions from land systems," *Sustainability Science*, vol. 1, no. 1, pp. 91–106, Oct. 2006.
- [5] Z. S. Zhou *et al.*, "Terrain slope correction and precise registration of SAR data for forest mapping and monitoring," in *International Symposium for Remote Sensing of the Environment*, pp. 1–4, Sydney, Australia, April 2011.
- [6] N. Campbell and X. Wu, "Gradient cross correlation for sub-pixel matching," in *Congress of the International Society for Photogrammetry and Remote Sensing*, vol. 7, pp. 1065–1070, Beijing, China, July 2008.
- [7] N. Campbell and W. Atchley, "The geometry of canonical variate analysis," *Systematic Zoology*, vol. 30, no. 3, pp. 268–280, Sep. 1981.
- [8] H. Kiiveri and N. Campbell, "Allocation of remotely sensed data using Markov models for image data and pixel labels," *Australian Journal of Statistics*, vol. 34, no. 3, pp. 361–374, Sep. 1992.
- [9] R. MacKay and N. Campbell, "Variable selection techniques in discriminant analysis – Description," *British Journal of Mathematical and Statistical Psychology*, vol. 35, no. 1, pp. 1–29, May. 1982.